stem cell-derived neuronal precursors. *J. Neurosci.* **15,** 5765–5778 (1995).
20. Altman, J. & Bayor, S. A. in *Development of the Cerebellar System in Relations to its Evolution, Structure and Functions* 727–750 (CRC, London, 1997).
21. Eilam, R. *et al.* Selective loss of dopaminergic nigro-striatal neurons in brains of Atm- deficient mice. *Proc. Natl Acad. Sci. USA* **95,** 12653–12656 (1998).
22. Spector, B. D., Filipovich, A. H., Perry, G. S. & Kersey, J. H. in *Ataxia-telangiectasia—A Cellular and Molecular Link Between Cancer, Neuropathology and Immune Deficiency* (eds Bridges, B. A. & Harnden, D. G.) 103–138 (Wiley, New York, 1982).
23. Rudolph, K. L. *et al.* Longevity, stress response, and cancer in aging telomerase-deficient mice. *Cell* **96,** 701–712 (1999).
24. Artandi, S. E. *et al.* Telomere dysfunction promotes non-reciprocal translocations and epithelial cancers in mice. *Nature* **406,** 641–645 (2000).
25. Tyner, S. D. *et al.* p53 mutant mice that display early ageing-associated phenotypes. *Nature* **415,** 45–53 (2002).
26. Greenberg, R. A. *et al.* Short dysfunctional telomeres impair tumorigenesis in the INK4a(delta2/3) cancer-prone mouse. *Cell* **97,** 515–525 (1999).
27. Smogorzewska, A. & de Lange, T. Different telomere damage signaling pathways in human and mouse cells. *EMBO J.* **21,** 4338–4348 (2002).
28. Frank, K. M. *et al.* DNA ligase IV deficiency in mice leads to defective neurogenesis and embryonic lethality via the p53 pathway. *Mol. Cell* **5,** 993–1002 (2000).
29. Sekiguchi, J. *et al.* Genetic interactions between ATM and the nonhomologous end-joining factors in genomic stability and development. *Proc. Natl Acad. Sci. USA* **98,** 3243–3248 (2001).
30. Wong, K. K. *et al.* Telomere dysfunction impairs DNA repair and enhances sensitivity to ionizing radiation. *Nature Genet.* **26,** 85–88 (2000).

Supplementary Information accompanies the paper on *Nature*'s website (**http://www.nature.com/nature**).

Acknowledgements We thank D. Castrillon and M. Bosenberg for advice on histo-pathological analyses, and S. Weiler, D. Castrillon, N. Sharpless, N. Bardeesy, C. Khoo and S. Chang for critical reading of the manuscript. K.-K.W. is a Howard Hughes Physician Postdoctoral Fellow. R.S.M. is supported by a Damon Runyon Cancer Research Fund Fellowship. R.M.B. and D.R.C. are both NIH Mentored Clinician Scientists awardees. F.W.A. is supported by the Howard Hughes Medical Institute. This work was supported by grants from the NIH and ACS to R.A.D. R.A.D. is an American Cancer Society Research Professor and a Steven and Michele Kirsch Investigator.

Competing interests statement The authors declare that they have no competing financial interests.

Correspondence and requests for materials should be addressed to R.A.D. (e-mail: ron_depinho@dfci.harvard.edu).

Plants lacking the main light-harvesting complex retain photosystem II macro-organization

A. V. Ruban*†, M. Wentworth*†, A. E. Yakushevska†‡, J. Andersson†§, P. J. Lee*, W. Keegstra‡, J. P. Dekker‖, E. J. Boekema‡, S. Jansson§ & P. Horton*

** Robert Hill Institute, Department of Molecular Biology and Biotechnology, University of Sheffield, Firth Court, Western Bank, Sheffield S10 2TN, UK*
‡ Biophysical Chemistry, Groningen Biomolecular Sciences and Biotechnology Institute, University of Groningen, Nijenborgh 4, 9747 AG Groningen, The Netherlands
§ Umeå Plant Science Centre, Department of Plant Physiology, Umeå University, S-901 87 Umeå, Sweden
‖ Faculty of Sciences, Division of Physics and Astronomy, Vrije Universiteit, De Boelelaan 1081, 1081 HV Amsterdam, The Netherlands
† These authors contributed equally to this work

Photosystem II (PSII) is a key component of photosynthesis, the process of converting sunlight into the chemical energy of life. In plant cells, it forms a unique oligomeric macrostructure in membranes of the chloroplasts[1]. Several light-harvesting antenna complexes are organized precisely in the PSII macrostructure—the major trimeric complexes (LHCII)[2] that bind 70% of PSII chlorophyll and three minor monomeric complexes[3]—which together form PSII supercomplexes[4–6]. The antenna complexes are essential for collecting sunlight and regulating photosynthesis[7–9], but the relationship between these functions and their molecular architecture is unresolved. Here we report that antisense *Arabidopsis* plants lacking the proteins that form LHCII trimers[10] have PSII supercomplexes with almost identical abundance and structure to those found in wild-type plants. The place of LHCII is taken by a normally minor and monomeric complex, CP26, which is synthesized in large amounts and organized into trimers. Trimerization is clearly not a specific attribute of LHCII. Our results highlight the importance of the PSII macrostructure: in the absence of one of its main components, another protein is recruited to allow it to assemble and function.

The central unit of PSII is the core complex, in which light is used to oxidize water to molecular oxygen, to reduce plastoquinone and to generate a transmembrane proton gradient[11,12]. In plants, each core dimer binds two copies of the minor, monomeric light-harvesting proteins CP29, CP26 and CP24 (the *Lhcb4*, *Lhcb5* and *Lhcb6* gene products, respectively) and two–four LHCII trimers (made up from the *Lhcb1*, *Lhcb2* and *Lhcb3* gene products) to form a PSII supercomplex[13,14]. Additional LHCII trimers have been located in membrane domains deficient in PSII supercomplexes, although they still can be involved in efficient light-harvesting[13]. These trimers consist of the *Lhcb1* and *Lhcb2* gene products[3], and can partition, depending on the phosphorylation state of LHCII, between the grana and stromal thylakoids to transfer energy to PSII and PSI, respectively[15,16].

This model for PSII macrostructure suggests that each light-harvesting protein has a unique position and role, but little is known about the structure–function relationships involved. In addition, the possibility cannot be excluded that there is some redundancy

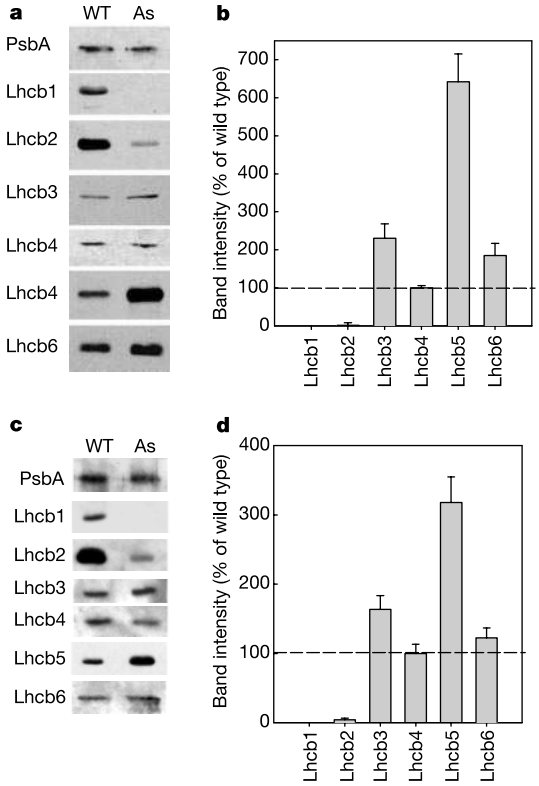

Figure 1 PSII membrane composition. **a**, **c**, Western blots of PSII membranes (**a**) and supercomplexes (**c**) prepared from wild-type (WT) and asLhcb2 (As) plants. Gels were probed with antibodies specific for the proteins indicated on the left. Sample loading was done on an equal chlorophyll basis. **b**, **d**, Results of densitometric analysis of the western blots of PSII membranes (**b**) and supercomplexes (**d**). Values are normalized to the amount of PsbA and are the means ± s.e.m. of four replicate gels.

among these similar light-harvesting proteins[17]. We have taken a genetic approach to investigating these complexes. Expression of a full-length *Lhcb2* antisense construct in *Arabidopsis thaliana* abolishes the expression of both *Lhcb2* and *Lhcb1*, owing to stretches of identical nucleotide sequences in these two genes[10]. The plants (called asLhcb2) are almost completely devoid of the two main proteins of trimeric LHCII, Lhcb1 and Lhcb2 (ref. 10). Western blot analysis of PSII membranes prepared from wild-type and asLhcb2 plants showed that Lhcb1 is completely absent and the amount of Lhcb2 is less than 5% of that found in wild type (Fig. 1a). When normalized to the amount of the PSII core protein PsbA, the quantities of Lhcb3, Lhcb4 and Lhcb6 were constant or less than twofold higher, whereas the amount of Lhcb5, the apoprotein of CP26, increased by more than sixfold (Fig. 1b).

The absorption spectra showed a strong reduction in the chlorophyll *b* band at 650 nm in the antisense membranes (Fig. 2a, curves 1 and 2), which is consistent with the measured chlorophyll *a*/*b* ratio of 4.3, as compared with 3.3 in the wild type, and is explained by the depletion of LHCII and the increase in CP26 (CP26 has a considerably higher chlorophyll *a*/*b* ratio than has LHCII[18]). The similarity between the fluorescence excitation spectrum and the absorption spectrum in both membranes (Fig. 2a, dotted lines) shows that the extra CP26 functions as an efficient light-harvesting antenna for PSII. Together with the identical photosynthetic activity of the wild-type and antisense plants[10], this indicates that PSII activity is the same in the wild-type and antisense plants.

Chromatographic analysis of detergent-solubilized PSII membranes[19] gave unexpected results. Fraction II, containing PSII supercomplexes, was still present in the antisense plants (Fig. 2b) but was highly enriched in CP26, containing over three times more Lhcb5 than present in the wild-type fraction (Fig. 1c, d). The quantity of Lhcb3 was also higher, whereas that of Lhcb4 and Lhcb6 was unchanged. These data indicate that the missing Lhcb1 and Lhcb2 in the supercomplex are replaced by CP26, which prompts an

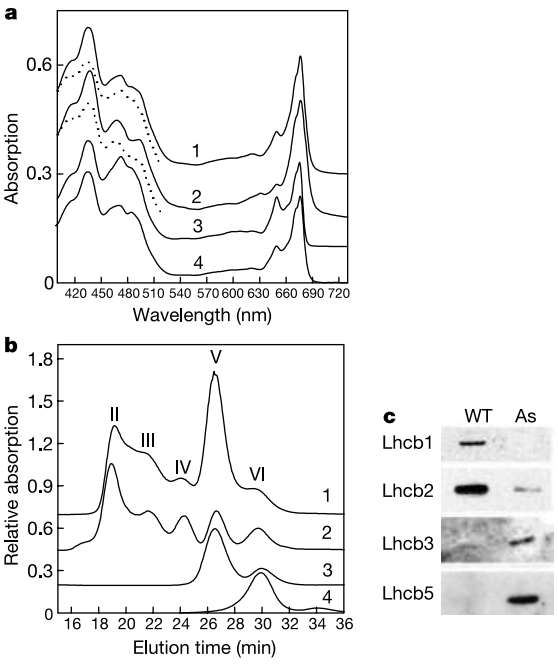

Figure 2 PSII membrane spectra. **a**, Absorption spectra of PSII membranes (curves 1 and 2) and gel-filtration fraction V (curves 3 and 4) prepared from wild-type (curves 1 and 3) and asLhcb2 (curves 2 and 4) plants. Dotted spectra show a fragment of the excitation spectrum of PSII fluorescence emission (685 nm) for the PSII membrane samples. **b**, Gel-filtration elution profiles of solubilized PSII membranes from wild-type (1) and asLhcb2 (2) samples, detected at 670 nm. The main fractions contain PSII supercomplexes (II), PSI (III), PSII cores (IV), trimeric light-harvesting complexes (V) and monomeric light-harvesting complexes (VI). Curves 3 and 4 show the elution profiles of purified LHCII trimers and a monomeric LHC fraction. **c**, Western blots of fraction V prepared from wild-type (WT) and asLhcb2 (As) plants. Details are as described in Fig. 1.

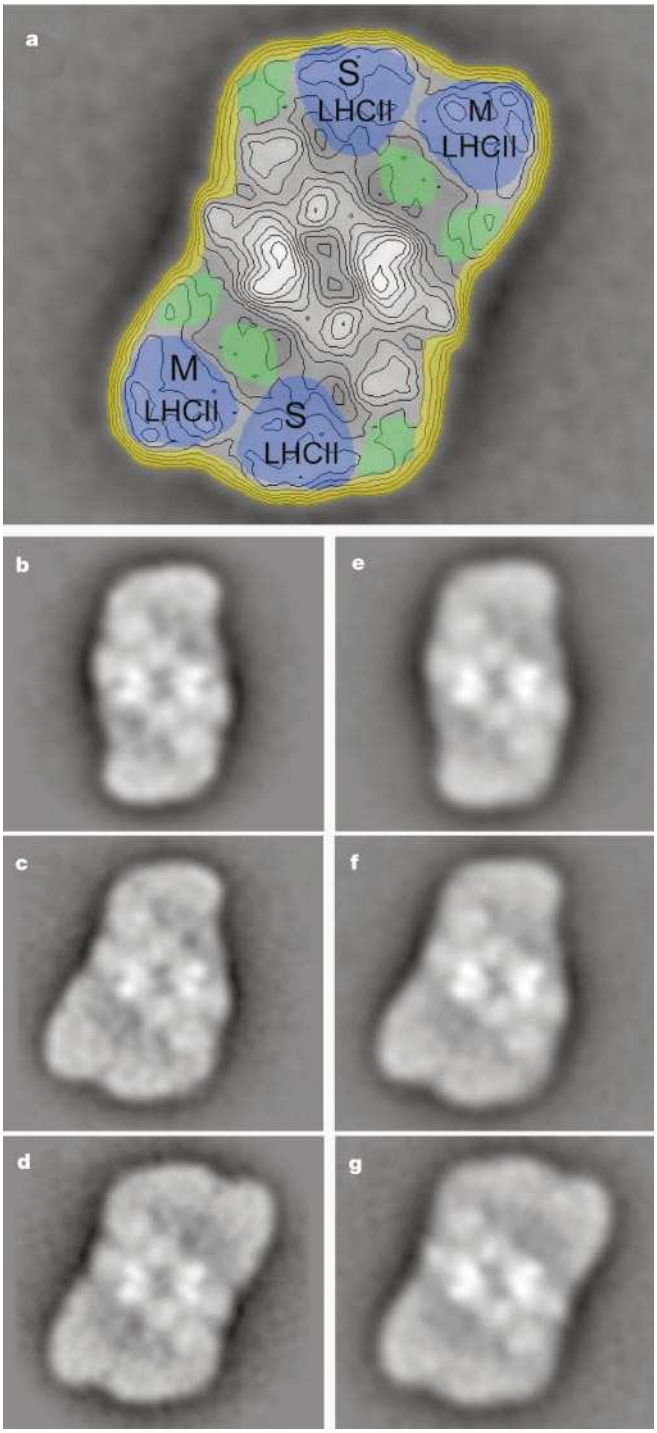

Figure 3 Average projections of the PSII complexes from *Arabidopsis* Lhcb2 plants. **a**, An *Arabidopsis* $C_2S_2M_2$ supercomplex[19] obtained previously, depicting the S- and M-LHCII trimers (blue), the monomeric complexes (green) and the detergent shell (yellow). **b**–**d**, Antisense Lhcb2 plants; **e**–**g**, wild-type plants. **b**, Average of 510 C_2S_2 projections; **c**, average of 290 C_2S_2M projections; **d**, average of 411 $C_2S_2M_2$ projections; **e**, average of 300 C_2S_2 projections; **f**, average of 948 C_2S_2M projections; **g**, average of 218 $C_2S_2M_2$ projections.

intriguing question: can CP26 assemble itself into a trimeric form to mimic the LHCII trimer? In fact, the gel-filtration separation procedure showed that a trimeric fraction (Fig. 2b, fraction V) was still present in the antisense plants, although its concentration was strongly reduced. Western blot analysis of this trimer showed that it contained only CP26 and Lhcb3 (Fig. 2c), whereas the wild-type fraction V contained almost exclusively Lhcb2 and Lhcb1, with some Lhcb3 (but at a much lower amount than in the antisense plant), as expected (refs 3, 7, and Fig. 2c).

The absorption spectra of the wild-type and antisense trimers were also clearly different (Fig. 2a (curves 3 and 4)), with reduced absorption at 650 nm from chlorophyll *b* in the antisense trimer. We calculated the chlorophyll *a*/*b* ratio of the wild-type trimer to be 1.4 as expected[2,3], but this ratio increased to 1.90–1.95 in the antisense plant. This higher ratio is explained by the chlorophyll *a*/*b* ratios of CP26 (2.0)[18], which we confirmed to be the same in the CP26 from both wild-type and antisense plants, and Lhcb3 (1.75)[20]. The ability to assemble into trimers *in vivo* was previously thought to be specific for Lhcb1 and Lhcb2. Clearly, this is not so.

Of all the other Lhc genes, *Lhcb5* bears the strongest sequence similarity to *Lhcb1* and *Lhcb2* (ref. 17), greater than 40%, as compared with roughly 30% or less for the other *Lhc* genes. *Lhcb5* is the only gene that clusters with the *Lhcb1–Lhcb3* genes[17]. In addition, a WYXXXR motif near the amino terminus of Lhcb1, which is necessary for LHCII trimerization[21], is conserved in Lhcb5, the apoprotein of CP26, but not in the apoproteins of CP29 and CP24. But another LHCII trimerization domain near the carboxy terminus (Trp 222)[22] is not found in Lhcb5, which could explain the reduced efficiency of trimerization for CP26.

We also analysed the isolated supercomplex population by electron microscopy and image analysis. The same three main classes of supercomplex[4] were found in both asLhcb2 (Fig. 3b–d) and wild-type (Fig. 3e–g) samples. Clearly, there are trimers lacking Lhcb1 and Lhcb2 that are assembled into the supercomplex in the antisense plants and, within the 2-nm resolution of the negative staining, are identical to those found in the wild type. Notably, the abundance of supercomplexes was about the same in both samples. Thus, they cannot arise from the residual Lhcb2 present in the antisense plants and cannot be due to Lhcb3, because the amount of this protein is not increased.

To find out how the supercomplexes are organized in the thylakoid membrane, electron microscopy was carried out on grana membrane fragments[13,19]. Ordered arrays of PSII supercomplexes were found in both wild-type and antisense plants (Fig. 4a, b). The frequency of occurrence of these arrays was judged to be about the same and, notably, the structural features were almost identical. Both images show arrays of PSII supercomplexes (Fig. 4b, red outline)[19]. In each one, rows of PSII cores (bright areas) are separated by areas of trimers, despite the absence in the antisense plants of the main proteins that are known to form LHCII trimers in the wild-type plants. The spacing between the rows is slightly reduced in the antisense plants, suggesting a slightly different packing of the complexes. Notably, also in the membranes from the antisense plants, the contours of the trimers are clearly apparent (Fig. 4a, arrows). Again, within the resolution of the technique, these trimers appear to be identical to those seen in the wild type.

These data show that the PSII supercomplexes have a precise molecular design in which trimers enable a normal supercomplex to be assembled and allow its correct organization in the thylakoid membrane. The observations that ordered arrays of PSII are formed in the antisense plants and that other proteins have been recruited to allow this formation show the importance of this feature of macromolecular organization of PSII. The plants attempt to compensate for the absence of LHCII by synthesizing more CP26 and assembling it into trimers, which then function as a PSII antenna and enable a normal macro-organization to be attained, including their grana structure[10]. This organization is essential for the high efficiency of energy usage in photosynthesis, because it allows energy exchange between PSII cores and energy migration over a large domain of chlorophyll molecules[23].

Because the wild-type supercomplex contains two CP26 copies for each dimeric PSII core complex, we estimate from the western blot analysis that the supercomplex from the antisense plants contains at least four additional copies of CP26 and up to two additional copies of Lhcb3. Thus, there is sufficient CP26 and Lhcb3 to form at least two trimers, thereby explaining how the structure of the complex can be virtually identical to the wild-type even though Lhcb1 and Lhcb2 are absent. In the PSII membranes, in which there is a sixfold increase in CP26, we estimate the presence of two further CP26-containing trimers, explaining the presence of $C_2S_2M_2$ supercomplexes.

The compensatory replacement of LHCII by CP26 does not give rise to a PSII unit of identical structure and function. There are small differences in the packing of the supercomplexes in the grana membrane but, more notably, the extra LHCII trimers per PSII not present in the supercomplex in wild-type plants[13] are apparently not replaced by CP26 in the antisense plants. Thus, there is a reduction in the total content of light-harvesting pigments. In addition, CP26 does not have the capacity to be phosphorylated,

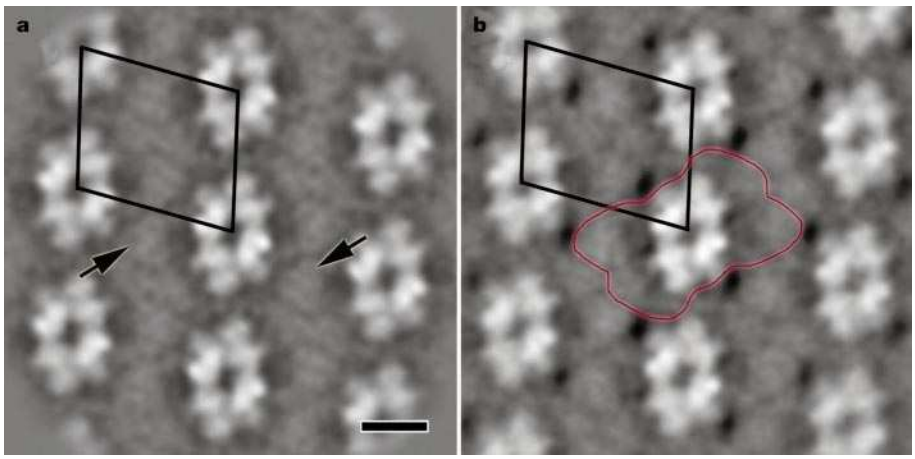

Figure 4 Final result of image analysis of two-dimensional crystalline PSII complexes from *Arabidopsis* wild-type and Lhcb2 antisense plants. **a**, Sum of 600 aligned crystal fragments from *Arabidopsis* Lhcb2 antisense plant with the unit cell (24.0 × 21.8 nm) and two trimers (arrows) indicated. **b**, Sum of 450 aligned crystal fragments from *Arabidopsis* wild-type with the unit cell (25.6 × 21.4 nm) and an outline of the fitting of the $C_2S_2M_2$ supercomplex (red line) indicated. Scale bar, 10 nm.

and therefore the antisense plants cannot carry out state transitions[10], a regulatory process that balances the excitation of the two photosystems and requires LHCII phosphorylation[15,16]. These two differences almost certainly account for the phenotype of these plants, the reduced fitness in the field[10] and the failure to grow normally under conditions of very low irradiance (J. Andersson and S. Jansson, unpublished data). Although there is some apparent redundancy between the similar Lhcb proteins, each one has specific features that confer its unique role in PSII structure and function. Lhcb1 and Lhcb2 are designed to form the essential trimeric building blocks of the supercomplex, where they form the major part of the PSII antenna, but they also provide the vital flexibility needed to regulate excitation distribution between the photosystems. When Lhcb1 and Lhcb2 are missing, CP26 can substitute but not completely. This explains why normally the precision of the composition of the supercomplexes is maintained absolutely in spite of this potential redundancy.

Do other membrane protein complexes show similar features? In cyanobacterial photosynthetic membranes, the CP43′ protein, which closely resembles the PSII core protein CP43, is synthesized under certain stress conditions and forms an oligomeric ring-like structure around PSI[24,25]. Thus, there are hitherto unrecognized features of the structure of macromolecular membrane protein complexes: the same or similar proteins may adopt different structural and functional roles in different or even the same complexes; and complexes that have the same overall structure may contain different proteins resulting in different functions. □

Methods

Plant growth

Arabidopsis thaliana cv. Columbia plants were grown in growth chambers with an 8-h photoperiod and 200 μmol quanta m^{-2} s^{-1} for 8 weeks as described[26]. The asLhcb2 line used shows almost total absence of the *Lhcb1* and *Lhcb2* gene products[10].

Sample preparation and analysis

PSII membranes were prepared as previously described[27], but with some modifications. In brief, leaves were homogenized three times for 5 s in a medium containing 20 mM Tricine-NaOH, pH 8.4, 0.45 M sorbitol, 10 mM EDTA and 0.1% bovine serum albumin. After pelleting and washing in 0.3 M sorbitol, 20 mM Tricine NaOH, pH 7.6, 5 mM $MgCl_2$, chloroplasts were osmotically shocked for 30 s with 5 mM $MgCl_2$, pH 7.6. Pelleted thylakoids were incubated in stacking medium (5 mM $MgCl_2$, 15 mM NaCl and 2 mM MES, pH 6.3) for 1 h, after which we treated them with 2.5% Triton X-100 at a chlorophyll concentration of 3 mg ml^{-1}. The PSII membranes were sedimented at 30,000*g* for 30 min, resuspended in buffer containing 20 mM Bis-Tris (pH 6.5) and 5 mM $MgCl_2$, and solubilized with 0.4% *n*-dodecyl-α-D-maltoside at a chlorophyll concentration of 1.4 mg ml^{-1}. Large fragments were removed by centrifugation for 3 min at 9,000 r.p.m. and the supernatant was filtered promptly through a 0.45-μm filter. Finally, the sample was subjected to gel-filtration chromatography using a Superdex 200 HR 10/30 column in an Amersham-Pharmacia Åcta Purifier system using the same buffer and similar conditions as before[19]. We prepared purified trimeric LHCII and monomeric LHC from spinach PSII membranes[28].

Spectroscopic analysis

Low-temperature spectroscopy was done using an Optistat^{DN} LN-2 cooled bath cryostat (Oxford Instruments). Samples were diluted in a medium containing 70% glycerol (w/v), 20 mM HEPES buffer, pH 7.8, 5 mM $MgCl_2$ and 0.33 M sorbitol. The chlorophyll concentration for absorption was 4 μM and for the fluorescence excitation measurements was 1 μM. A poly(methyl metacrylate) PMMA 1-cm cuvette was used for all experiments. Absorption measurements were carried out using a Cary 500 UV-Vis-NIR spectrophotometer and corrected fluorescence exciation spectra were recorded using a SPEX FluoroLog FL3-22 spectrofluorimeter.

Electrophoresis and western blot analysis

Protein samples were solubilized and separated by 15% denaturing SDS–PAGE essentially as described[29]. Roughly equal amounts of chlorophyll were loaded, about 2 μg per lane for PSII membranes and 0.5 μg for isolated supercomplexes and trimers. Proteins were transferred to Hybond-P PVDF membrane (Amersham Pharmacia) in a Mini-Trans-Blot transfer cell (Bio-Rad) at 30 mA for 12 h. Membranes were detected with specific antibodies against the proteins Lhcb1–Lhcb6 (ref. 30) and PsbA (a gift from P. Nixon). The primary antibody was detected by a horseradish peroxidase (HRP)-labelled secondary antibody using an ECL Plus kit (Amersham Pharmacia). Chemiluminesence was detected on Hyperfilm ECL (Amersham Pharmacia) photographic film. We developed the films for 20 min, dried and digitized them in 256-bit greyscale at a resolution of 600 d.p.i. using an Umax Powerlook III high-resolution scanner set in transmission mode. (Films were developed for 0.5–60 min and densities were found to be linear over the first 40 min for each antibody.) A standard Kodak photographic 21 step tablet (OD 0.05–3.05) was used to calibrate the scanner each time an image was scanned. We processed images using the 1D software package of the Image Master Suite (Amersham Pharmacia). Individual lanes and bands were detected automatically by the software, and background for each lane was subtracted using the rolling disc option to give the final band density. For the antibodies against Lhcb1, Lhcb2 and Lhcb5, linear densitometric responses were found in the range of 0.5–10 μg of chlorophyll per lane for PSII membranes.

Electron microscopy

After chromatography, fractions were immediately prepared for electron microscopy. Samples were negatively stained using the droplet method with 2% uranyl acetate and were prepared on glow discharge carbon-coated copper grids as described[4]. The membrane fragments and supercomplexes were analysed by a similar method to that used for preparations from spinach and the wild-type *Arabidopsis* plants[13,19]. The samples were imaged in a Philips CM10 electron microscope at × 52,000 magnification. Electron micrographs were digitized with a Kodak Eikonix Model 1412 CCD (charge-coupled device) camera. Single-particle projections were extracted from negatives and analysed with IMAGIC software (Image Science Software GmbH) and Groningen Image Processing ('GRIP') software (Groningen University Software)[13,19].

Received 22 August; accepted 3 December 2002; doi:10.1038/nature01344.

1. Hankamer, B., Barber, J. & Boekema, E. J. Structure and membrane organisation of photosystem II in green plants. *Annu. Rev. Plant Physiol. Plant Mol. Biol.* **48,** 641–671 (1997).
2. Kühlbrandt, W. & Wang, D. N. Three dimensional structure of plant light-harvesting complex by electron crystallography. *Nature* **350,** 130–134 (1991).
3. Peter, G. F. & Thornber, J. P. Biochemical composition and organization of higher plant photosystem II light-harvesting pigment-proteins. *J. Biol. Chem.* **266,** 16745–16754 (1991).
4. Boekema, E. J., Van Roon, H., Calkoen, F., Bassi, R. & Dekker, J. P. Multiple types of association of photosystem II and its light-harvesting antenna in partially solubilized photosystem II membranes. *Biochemistry* **38,** 2233 (1999).
5. Boekema, E. J., Van Roon, H., Van Breemen, J. F. L. & Dekker, J. P. Supramolecular organization of photosystem II and its light-harvesting antenna in partially solubilized photosystem II membranes. *Eur. J. Biochem.* **266,** 444–452 (1999).
6. Nield, J., Orlova, E. V., Morris, E. P., Gowen, B., Van Heel, M. & Barber, J. 3D map of the plant photosystem II supercomplex obtained by cryoelectron microscopy and single particle analysis. *Nature Struct. Biol.* **7,** 44–47 (2000).
7. Jansson, S. The light-harvesting chlorophyll *a*/*b*-binding proteins. *Biochim. Biophys. Acta* **1184,** 1–19 (1994).
8. Paulsen, H. Chlorophyll *a*/*b* binding proteins. *Photochem. Photobiol.* **62,** 367–382 (1995).
9. Horton, P., Ruban, A. V. & Walters, R. G. Regulation of light harvesting in green plants. *Annu. Rev. Plant Physiol. Plant Mol. Biol.* **47,** 655–684 (1996).
10. Andersson, J. *et al.* Absence of the main light harvesting complex of photosystem II affects photosynthetic function. *Plant J.* (in the press).
11. Barber, J. Photosystem II: a multisubunit membrane protein that oxidizes water. *Curr. Opin. Struct. Biol.* **12,** 523–530 (2002).
12. Zouni, A. Crystal structure of photosystem II from *Synechoccus elongatus* at 3.8 Å resolution. *Nature* **409,** 739–743 (2001).
13. Boekema, E. J., Van Breemen, J. F. L., Van Roon, H. & Dekker, J. P. Arrangement of photosystem II in crystalline macrodomains within the thylakoid membrane of green plant chloroplasts. *J. Mol. Biol.* **301,** 1123–1133 (2000).
14. Hankamer, B. *et al.* Isolation and characterization of monomeric and dimeric photosystem II complexes from spinach and their relevance to the organisation of photosystem II *in vivo*. *Eur. J. Biochem.* **243,** 422–429 (1997).
15. Allen, J. F. & Forsberg, J. Molecular recognition in thylakoid structure and function. *Trends Plant Sci.* **6,** 317–326 (2001).
16. Haldrup, A., Jensen, P. E., Lunde, C. & Scheller, H. V. Balance of power: a view of the mechanism of photosynthetic state transitions. *Trends Plant Sci.* **6,** 301–305 (2001).
17. Jansson, S. A guide to the *Lhc* genes and their relatives in *Arabidopsis*. *Trends Plant Sci.* **4,** 236–240 (1999).
18. Croce, R., Canino, G., Ros, F. & Bassi, R. Chromophore organisation in the higher plant photosystem II antenna protein CP26. *Biochemistry* **41,** 7334–7343 (2002).
19. Yakushevska, A. E. *et al.* Supramolecular organisation of photosystem II and its associated light harvesting antenna in *Arabidopsis thaliana*. *Eur. J. Biochem.* **268,** 6020–6028 (2001).
20. Caffrari, S., Croce, R., Cattivelli, L. & Bassi, R. The Lhcb1, 2 and 3 gene products, components of the trimeric antenna complex of higher plant photosystem II, have distinct biochemical and spectroscopic properties. *Proc. 12th Int. Congr. Photosyn.*, S31–034 (CSIRO, Canberra, 2001).
21. Hobe, S., Foster, R., Klingler, J. & Paulsen, H. N-proximal sequence motif in light-harvesting chlorophyll-*a*/*b*-binding protein is essential for trimerisation of the light harvesting chlorophyll *a*/*b* complex. *Biochemistry* **34,** 10224–10228 (1995).
22. Kuttkat, A., Kartmann, A., Hobe, S. & Paulsen, H. The C-terminal domain of light-harvesting chlorophyll-*a*/*b*-binding protein is involved in the stabilisation of trimeric light harvesting complex. *Eur. J. Biochem.* **242,** 288–292 (1996).
23. Garab, G. & Mustardy, L. Role of LHCII-containing macrodomains in the structure, function and dynamics of grana. *Aust. J. Plant Physiol.* **27,** 648–658 (1999).
24. Bibby, T., Nield, J. & Barber, J. Iron deficiency induces the formation of an antenna ring around trimeric photosystem I in cyanobacteria. *Nature* **412,** 743–745 (2001).
25. Boekema, E. J. *et al.* A giant chlorophyll-protein complex induced by iron deficiency in cyanobacteria. *Nature* **412,** 745–748 (2001).
26. Walters, R. G., Rogers, J. J. M., Shephard, F. & Horton, P. Acclimation of *Arabidopsis thaliana* to the light environment: the role of photoreceptors. *Planta* **209,** 517–527 (1999).
27. Berthold, D. A., Babcock, G. T. & Yocum, C. F. A highly resolved, oxygen-evolving photosystem II preparation from spinach thylakoid membranes. EPR and electron transport properties. *FEBS Lett.* **134,** 231–234 (1981).

28. Ruban, A. V., Lee, P. J., Wentworth, M., Young, A. J. & Horton, P. Determination of the stoichiometry and strength of binding of xanthophylls to the photosystem II light harvesting complexes. *J. Biol. Chem.* **274,** 10458–10465 (1999).
29. Laemmli, U. K. Cleavage of structural proteins during the assembly of the head of bacteriophage T4. *Nature* **227,** 680–685 (1970).
30. Andersson, J., Walters, R. G., Horton, P. & Jansson, S. Antisense inhibition of the photosynthetic antenna proteins CP29 and CP26: implications for the mechanism of protective energy dissipation. *Plant Cell* **13,** 1193–1204 (2001).

Acknowledgements We wish to thank R. Walters for discussions. This work was supported by the UK Biotechnology and Biological Sciences Research Council, the UK Joint Infrastructure Fund, the Netherlands Foundation for Scientific Research (NWO) through the Foundation for Life and Earth Sciences (ALW), and the Swedish Research Council for Environment, Agricultural Sciences and Spatial Planning and the Foundation for Strategic Research.

Competing interests statement The authors declare that they have no competing financial interests.

Correspondence and requests for materials should be addressed to P.H. (e-mail: p.horton@sheffield.ac.uk).

Structure and catalytic mechanism of the human histone methyltransferase SET7/9

Bing Xiao*, Chun Jing*, Jonathan R. Wilson*, Philip A. Walker*, Nishi Vasisht*, Geoff Kelly*, Steven Howell*, Ian A. Taylor*, G. Michael Blackburn† & Steven J. Gamblin*

* *Structural Biology Group, National Institute for Medical Research, Mill Hill, London NW7 1AA, UK*
† *Department of Chemistry, Krebs Institute, University of Sheffield, Sheffield S3 7HF, UK*

Acetylation[1,2], phosphorylation[3] and methylation[4] of the amino-terminal tails of histones are thought to be involved in the regulation of chromatin structure and function[5–7]. With just one exception[8,9], the enzymes identified in the methylation of specific lysine residues on histones (histone methyltransferases) belong to the SET family[10]. The high-resolution crystal structure of a ternary complex of human SET7/9 with a histone peptide and cofactor reveals that the peptide substrate and cofactor bind on opposite surfaces of the enzyme. The target lysine accesses the active site of the enzyme and the *S*-adenosyl-L-methionine (AdoMet) cofactor by inserting its side chain into a narrow channel that runs through the enzyme, connecting the two surfaces. Here we show from the structure and from solution studies that SET7/9, unlike most other SET proteins, is exclusively a mono-methylase. The structure indicates the molecular basis of the specificity of the enzyme for the histone target, and allows us to propose a model for the methylation reaction that accounts for the role of many of the residues that are invariant across the SET family.

Many SET proteins have now been characterized biochemically and several have been the subject of X-ray structure analysis: SET7/9 from human[11] and its complex with the product *S*-adenosyl-L-homocysteine (AdoHcy)[12]; Dim-5 from *Neurospora crassa*[6]; Rubisco large subunit methyltransferase (LSMT) from pea with AdoHcy[13]; and Clr4 from *Schizosaccharomyces pombe*[14]. SET proteins can be classified according to the lysine residues that they target on histones H3, H4 and H2A[4], and it is apparent that methylation at these different sites gives rise to distinct biological effects. An additional level of complexity is that lysine residues may be mono-, di- or tri-methylated and that these distinct species lead to different signalling events. For example, in *Saccharomyces cerevisiae*, although di-methylation of Lys 4 on histone H3 is present at both active and inactive euchromatic genes, tri-methylation is linked exclusively to active genes[15].

NMR studies (see Supplementary Information) indicated that a histone peptide containing mono-methylated Lys 4 was better ordered in complex with SET7/9 than unmodified peptide. We therefore used the products of the normal histone methyltransferase (HMT) reaction for crystallization experiments (methylated lysine peptide and AdoHcy). In our previous studies[11] we obtained useful SET7/9 crystals only from constructs lacking the small carboxy-terminal segment, which is, nevertheless, essential for the catalytic activity of the enzyme. Here, we have used a catalytically active construct that contains the complete C-terminal segment. We obtained well-ordered crystals of the ternary complex of SET7/9 that diffracted to at least 1.7 Å spacing, and the structure was readily solved by molecular replacement. The C-terminal segment, the AdoHcy cofactor and most of the substrate peptide are well defined in the electron density maps, as are all the important residues around the active site. The overall structure of the ternary complex

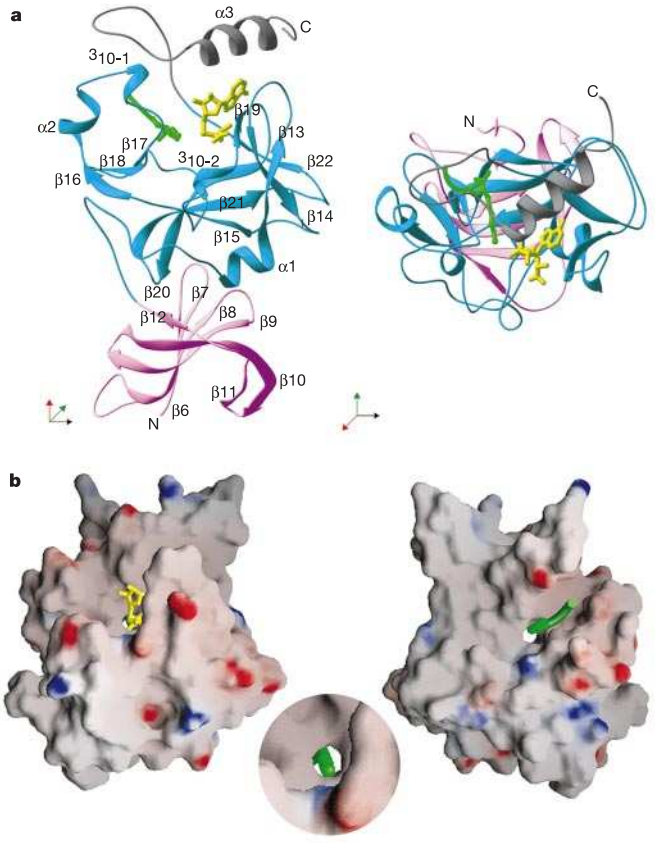

Figure 1 Structure of the SET7/9 ternary complex. **a**, Two orthogonal views of the SET7/9 ternary complex in ribbons representation. The N-terminal domain is coloured pink, the SET domain is blue and the C-terminal segment is grey. The H3 peptide is indicated in green, with the side chain of methylated Lys 4 shown. The *S*-adenosyl-L-homocysteine (AdoHcy) cofactor is coloured yellow. The secondary structure elements are labelled according to our earlier structure. Two small turns of the 3_{10} helix are also labelled. **b**, Two views of the SET domain are shown in a surface representation coloured according to electrostatic potential (the two views are related by a twofold rotation about a vertical axis). The left panel shows AdoHcy coloured yellow; the right panel shows the H3 peptide coloured green. The inset panel shows a close-up view of the lysine access channel containing the methyl lysine side chain as viewed from the *S*-adenosyl-L-methionine (AdoMet)-binding site.

